

Collider Inclusive Jet Data and the Gluon Distribution

Jon Pumplin^a, J. Huston^a, H. L. Lai^b, P. M. Nadolsky^d, Wu-Ki Tung^{a,c,e} and C.-P. Yuan^a

^a*Michigan State University, East Lansing, Michigan*

^b*Taipei Municipal University of Education, Taipei, Taiwan*

^c*University of Washington, Seattle, Washington; ^eDeceased*

^d*Department of Physics, Southern Methodist University, Dallas, Texas*

(Dated: November 3, 2018)

Inclusive jet production data are important for constraining the gluon distribution in the global QCD analysis of parton distribution functions. With the addition of recent CDF and D0 Run II jet data, we study a number of issues that play a role in determining the up-to-date gluon distribution and its uncertainty, and produce a new set of parton distributions that make use of that data. We present in detail the general procedures used to study the compatibility between new data sets and the previous body of data used in a global fit. We introduce a new method in which the Hessian matrix for uncertainties is “redagonalized” to obtain eigenvector sets that conveniently characterize the uncertainty of a particular observable.

1. INTRODUCTION

The gluon distribution $g(x, \mu)$ plays an important role in high energy collider phenomenology, both for standard model and new physics. Yet it is the most elusive of the parton distribution functions (PDFs) in contemporary global QCD analysis. At moderate values of the momentum fraction x , extensive high precision data on deep inelastic scattering (DIS) constrain $g(x, \mu)$ fairly well through the μ -dependence that is predicted by QCD. The little information we have at large x comes mostly from inclusive jet production at hadron colliders, which receives contributions directly from the gluon distribution at leading order in α_s . The recently published inclusive jet data from Tevatron Run II measurements by CDF [1] and D0 [2] are therefore of considerable interest for improving our knowledge of the gluon distribution.

Previous CTEQ studies [4, 5] have used only the Run I jet data [7, 8]. A recent MSTW study [6] includes the Run II data in an analysis with aims parallel to this one. A comparison with their results is presented in Sec. 8.

In this paper, we make a detailed study of several issues that bear on the behavior of the gluon distribution and its range of uncertainties, focusing on the use of Tevatron inclusive jet data. (Inclusive jet production in DIS processes can also provide constraints on the gluon distribution; but those constraints are considerably weaker and we do not include them here.) Some of the results and techniques described here are known to many practitioners in the field, but have not been previously documented in the literature. Some of these results are frequently misunderstood—e.g., in discussions at workshops—so it seems worthwhile to set them out in systematic detail. The methods dis-

cussed here for the inclusive jet data thus serve as a pedagogical study of techniques that can be applied in general when new data sets become available to advance the PDF analysis.

One of the techniques we use is presented here for the first time. It involves orienting the choice of eigenvector directions in the Hessian method in order to simplify the study of uncertainty for any particular quantity of interest.

2. THEORY CALCULATIONS FOR INCLUSIVE JETS

Up to now, the CTEQ global analyses of jet cross sections as a function of jet transverse momentum p_T have been based on the EKS NLO program [9]. Recently, the FastNLO implementation [10] of the NLO-JET++ [11] calculation has gained increasing use—in part because of its convenient interface. (FastNLO allows the dependence on the PDFs of the NLO cross section to be included in the computation of χ^2 at every step within the fitting procedure. However, we find that calculating the ratio $K=NLO/LO$ for each data point using a single typical fit to the data provides an adequate approximation.) To make sure that the two calculations are consistent in the global analysis context, we have directly compared their results in the Tevatron Run I and II kinematic ranges. The theoretical results also depend on choices of: (i) the renormalization and factorization scales in PQCD, usually taken to be the same, say μ ; and (ii) the jet algorithm, including parameters such as R_{sep} (for separation of neighboring jets) [1]. We have performed the comparison using a variety of these choices. The results provide information on the importance of these factors for

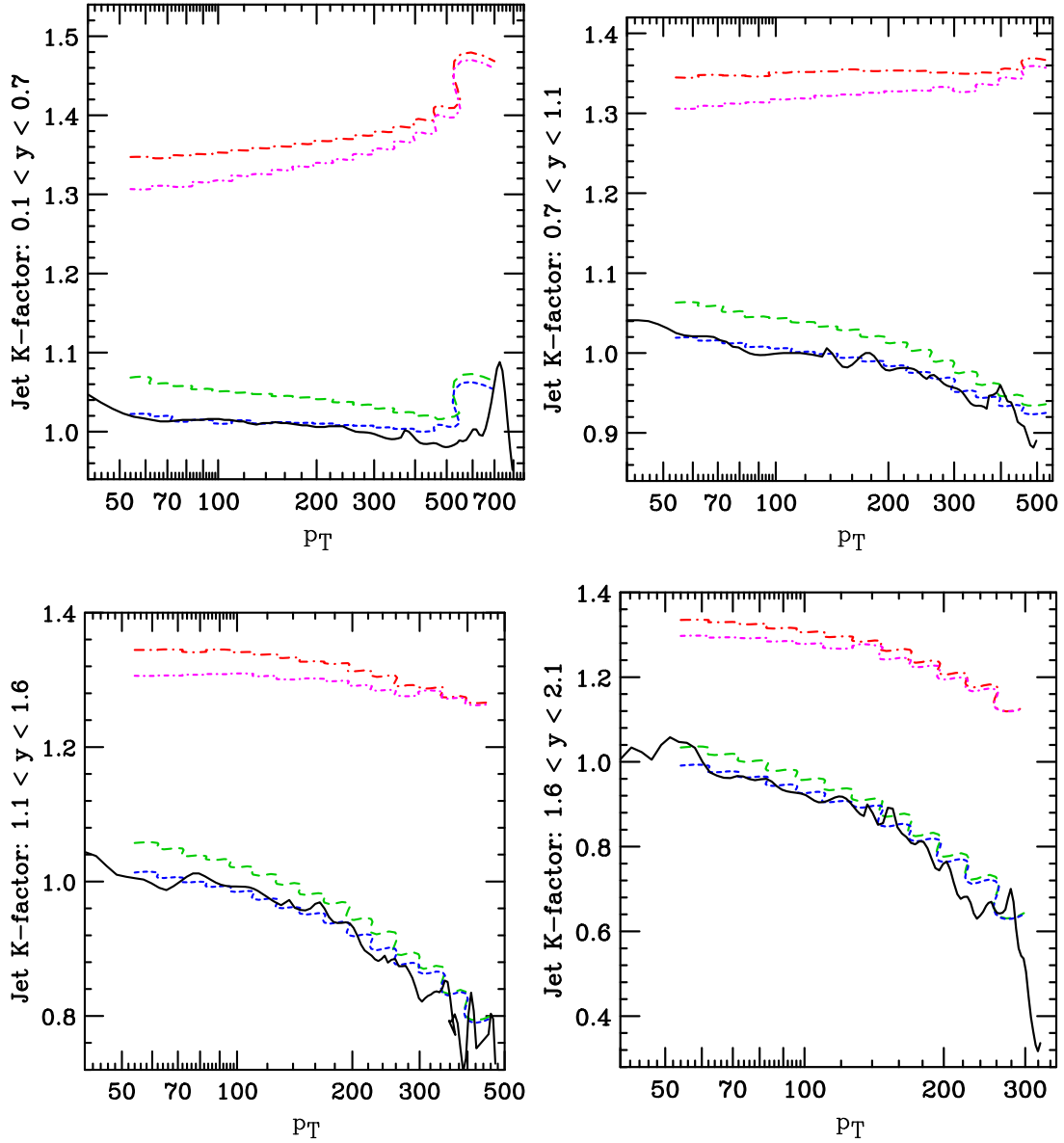


FIG. 1: Theory calculations for the ratio $K = \text{NLO}/\text{LO}$ from FastNLO and EKS. FastNLO with $\mu = p_T$: $R_{\text{sep}} = 2.0$ (long dash dot), $R_{\text{sep}} = 1.3$ (short dash dot); FastNLO with $\mu = p_T/2$: $R_{\text{sep}} = 2.0$ (long dash), $R_{\text{sep}} = 1.3$ (short dash); EKS with $\mu = p_T/2$, $R_{\text{sep}} = 1.3$ (solid).

the global analysis.

Figure 1 shows the K-factor, defined by $K = \text{NLO}/\text{LO}$, for the Tevatron Run II p_T range in several of the experimental rapidity intervals. Each plot shows results from FastNLO for two choices of the scale: $\mu = p_T$ (upper two curves), and $\mu = p_T/2$ (lower two dashed curves). Within each of these pairs, the upper curve uses the midpoint cone jet algorithm with $R_{\text{sep}} = 2.0$, while the lower curve uses the midpoint al-

gorithm with $R_{\text{sep}} = 1.3$. The solid curve shows the result of the EKS program for $\mu = p_T/2$ and $R_{\text{sep}} = 1.3$. (The wiggles in this curve are caused by fluctuations from the Monte Carlo integration used in EKS.) We observe the following:

- The overall agreement between the EKS and FastNLO calculations is satisfactory, though not perfect. Our results from parallel global analyses based on these two methods for calculating jets, with all other

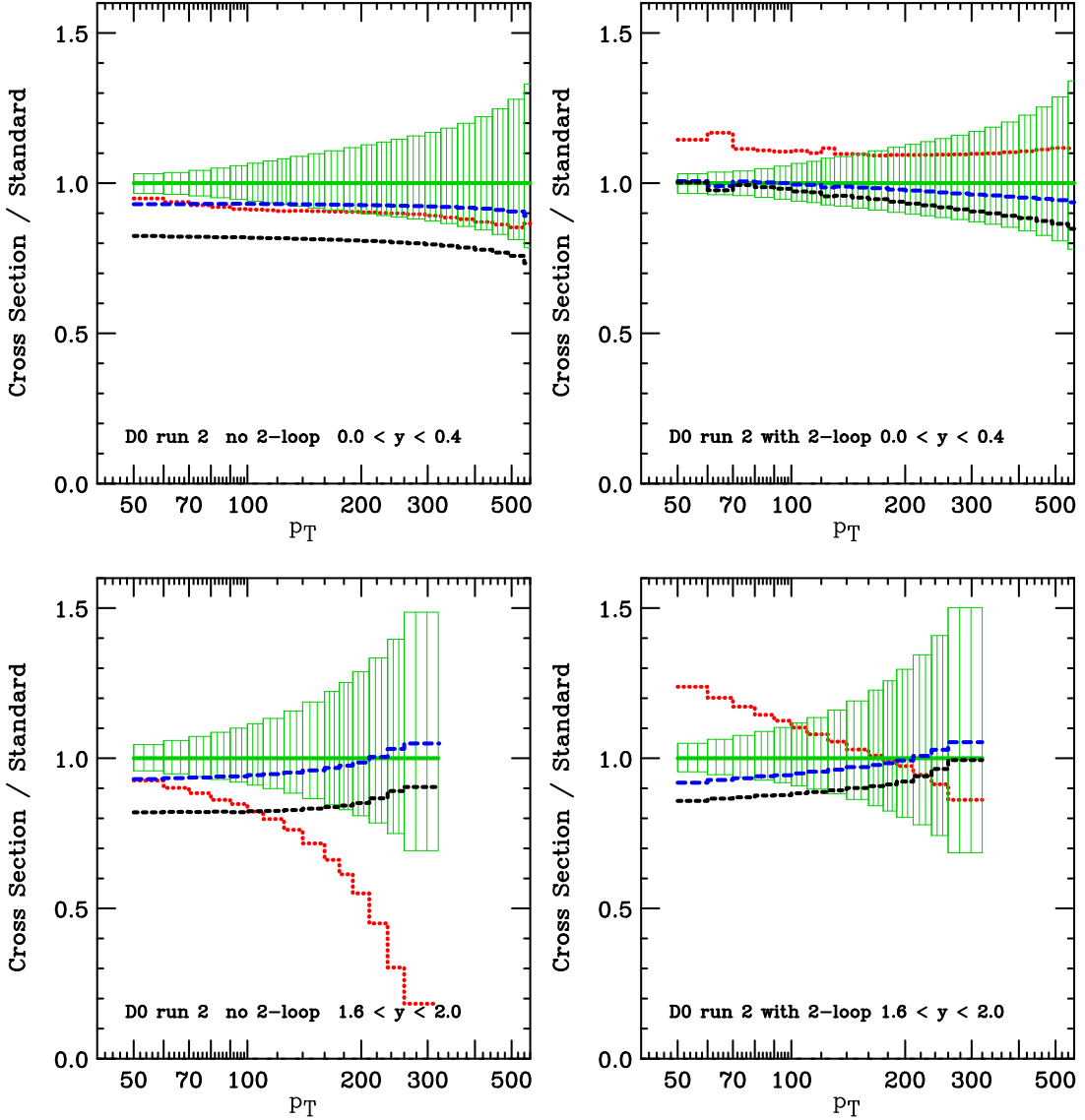


FIG. 2: Effect of scale choice on predicted cross section with $R_{\text{sep}} = 1.3$: $\mu = 2p_T$ (short dash), p_T (long dash), $p_T/2$ (solid), $p_T/4$ (dotted), relative to our Standard Choice ($\mu = p_T/2$, $R_{\text{sep}} = 1.3$, no “two-loop” correction). Right panels include the “two-loop” resummation correction. Uncertainty bands from PDFs are shown for comparison.

options identical, show good agreement, which indicates that results of the global analysis are not sensitive to deviations of the magnitude shown. We use the FastNLO results for the remainder of this investigation.

- The effect of R_{sep} choice is quite small.

Since the scale choice affects the predicted cross section directly through the LO cross section, as well as through the K factor, we explore it further in Fig. 2, which shows the predicted cross section for vari-

ous scale choices normalized by our “standard” choice. The plots on the left correspond to the conventional NLO calculation, while those on the right also include a “2-loop” correction derived from threshold resummation [12], which is available in FastNLO. We only show results from one central and one large rapidity bin; results at intermediate y interpolate between these two. The bands in each plot represent the estimated uncertainty due to the PDFs, for comparison. We conclude the following:

- The low-scale choice $\mu = p_T/4$ leads to results that are far from the other choices at large rapidity, and shows unstable behavior with respect to 2-loop corrections, which lie mostly outside the PDF uncertainty bands. This scale choice is thus unsuitable for theoretical calculations, as is also apparent from the fact that $K = \text{NLO}/\text{LO}$ is far from 1 with this choice, which suggests that still higher order corrections would be very important. By contrast, the other three scale choices show consistent patterns and yield stable results.
- One may use the range $p_T/2 < \mu < 2p_T$ to empirically estimate the uncertainty due to uncalculated higher-order corrections. This range of theoretical uncertainty is seen to be fairly independent of p_T , in contrast to the uncertainty due to PDFs, which has a strong p_T dependence. The theory uncertainty is comparable to the PDF uncertainty in the low p_T range, but is much smaller than it in the high p_T range.
- The theoretical uncertainties are reduced in the calculation that includes the partial 2-loop correction. Whether this reduction provides a genuine increase in accuracy depends on the reliability of the approximation, which is still controversial. We do not use this correction in the remainder of the paper.

With these theoretical background studies completed, we now proceed to study the impact of the Tevatron jet data on determining the gluon distribution.

3. PRELIMINARY GLOBAL FIT WITH THE NEW JET DATA

We use the published CTEQ6.6 PDF set [5] as the reference fit for our comparison study. Unless otherwise stated, the theoretical and experimental inputs are kept the same as in [5] except for the addition of the CDF [1] and D0 [2] Run II data sets.

We use the CDF Run II results obtained from the midpoint cone jet algorithm, rather than the earlier results based on the k_T algorithm [3]. The two analyses were carried out on the same events, so it be incorrect to include them both; and the ratio of the resulting cross sections agrees well with the ratio predicted by NLO QCD, as stated in [1]. (The CDF data were supplied to us by one of the CDF authors, so we were not affected by errors in the original publication [1], which have now been corrected as described in its first reference.)

The CTEQ6.6 central fit and its eigenvector sets which characterize the uncertainty are known to describe the Run II jet data fairly well, even though those

data were not available at the time of the CTEQ6.6 analysis. Thus from the outset we know that no revolutionary changes will result from incorporating the new data into the global analysis. The purpose of our study is to quantify what changes there are; and to investigate some subtle features that have not been explored before, which have implications for our efforts to pin down the gluon PDF.

With the addition of the Tevatron Run II jet data, our global analysis includes 37 data sets with a total of 2898 data points. As a baseline, when CTEQ6.6 PDFs are used directly to compute the cross sections and then compared to these data points, we obtain a good overall fit with $\chi^2 = 2756$. *Here and in all our fits, the full correlated experimental errors are used in computing χ^2 , for all experiments that report their errors in this form.* To get a first look at the impact of the Run II jet data, we performed a preliminary fit using the same theoretical input as CTEQ6.6. In this fit, the weighted χ^2 becomes 2740—a reduction of 16. This is a very small reduction when spread over all 2898 data points, or even when spread over the 182 new ones—as was anticipated since CTEQ6.6 already provided a reasonably good fit to the new data.

The only significant change in the best-fit PDFs from CTEQ6.6 to the preliminary fit occurs in the gluon PDF. This can be demonstrated by repeating the global fit with all of the quark distribution parameters frozen at their CTEQ6.6 values, thus only allowing the gluon distribution to change. The reduction in χ^2 is nearly the same and the resulting fit is essentially equivalent to the preliminary fit. This confirms our expectation that the inclusive jet data provide a handle on $g(x, \mu)$ and little else.

4. PARAMETRIZING THE GLUON DISTRIBUTION

Since the jet data are sensitive to the gluon distribution, it is essential to use a sufficiently flexible parametrization for the gluon at the starting scale μ_0 for DGLAP evolution, which we choose to be 1.3 GeV as in previous analyses. The form we use is

$$g(x, \mu_0) = a_0 x^{a_1} (1-x)^{a_2} \exp(a_3 x + a_4 x^2 + a_5 \sqrt{x}). \quad (1)$$

We add a penalty to the overall χ^2 to force parameter a_2 , which controls the behavior at $x \rightarrow 1$, to lie within a reasonable but generous range $0.5 \lesssim a_2 \lesssim 10$. The form (1) is more general than what was used in CTEQ6.6, which was equivalent to $a_2 = 4$ and $a_5 = 0$. Alternative parametrizations have also been tested, to assure that our results are not sensitive to the particu-

lar form of smooth function that we choose to multiply the basic x^{a_1} and $(1-x)^{a_2}$ factors.

Because the gluon distribution is not strongly constrained by existing data, it has been common to use a fairly restricted functional form for the non-perturbative input function, compared to the better-constrained light quark distributions. A frequent practice is to start with the minimal form $x^{a_1}(1-x)^{a_2}$ and incrementally add new parameters until the quality of the global fit ceases to improve. This is a sensible approach for finding a reasonable “best fit” PDF set. But it can produce misleading results by artificially reducing the estimated uncertainties—as happened famously when the CDF Run I measurements of the jet cross section at first appeared to lie outside the range of standard model predictions at large p_T [13, 14]. We will discuss related examples of this in Secs. 5.1 and 7.

In current practice, the number of parameters used by various groups shows wide variation, which depends both on the constraining power of the input experiments included in the analysis and on the stability of the analysis method. Using too few parameters can lead to uncertainty estimates that reflect the assumed functional forms more than the experimental constraints. This fact appears to be underappreciated, since the number of parameters used for uncertainty studies is commonly kept at a minimum level based only on the central fit.

A technical reason to restrict the number of parameters in the uncertainty study is the instability of the Hessian method for determining the extreme PDF eigenvector sets, which occurs as the number of fitting parameters approaches the limit of constraining power of the experimental input. We have been able to overcome this problem by using the iterative method developed in [15] to control both the instabilities due to vast disparities in the unscaled eigenvalues and instabilities caused by the numerical evaluation of the second derivatives that define the Hessian matrix. The set of tools we have developed provide an orderly way to obtain stable results as the number of parameters is increased. This is the reason why the CTEQ analyses have consistently used a larger number of uncertainty eigenvector sets than other groups. The fits described in Sec. 7 use 24 parameters to describe the PDFs at μ_0 .

A Neural Network approach to the PDF analysis (NNPDF) [16] has been developed recently to circumvent the parametrization issue. This appears highly promising. However, to make this approach as effective as possible, it may be important to retain some theory-based guidelines on the PDFs at scale μ_0 . In particular, there are good physical arguments behind

the traditionally assumed behaviors x^{a_1} at $x \rightarrow 0$ and $(1-x)^{a_2}$ at $x \rightarrow 1$, which even predict estimates for the constants a_1 and a_2 that one may wish to harness. The validity of those arguments is supported by the observation that for the u quark distribution, which is the most accurately measured of the PDFs, the fitted results for a_1 and a_2 lie close to their theoretical expectations.

We now proceed to a detailed study of the compatibility of the jet data sets with each other and with the nonjet data. This study also serves as a case study of methods to apply when adding new data sets to a global fit.

5. TESTING COMPATIBILITY OF DATA SETS USING WEIGHTED χ^2

When one contemplates adding new sets of experimental data to an existing global analysis, one begins by asking a series of questions that can be answered systematically by making fits in which the χ^2 for the new data sets are multiplied by various weight factors. These weight factors multiply the contributions from individual data sets before they are added to the global χ^2 that is minimized in the fit, in order to vary how much influence each set is allocated in determining the fit. For a related discussion of these ideas, see [17].

Are the new data consistent with theory? can be addressed in a minimal way by seeing if χ^2 for the new data is acceptably close to its nominal range of $N \pm \sqrt{2N}$ for N data points, at least when these data are assigned a sufficiently large weight. (In the ideal situation of Gaussian experimental errors, this range corresponds to a 1σ confidence interval around the best-fit χ^2 . In the present case, where the bulk of the experimental error may come from systematic effects, this comparison may also reveal deviations from Gaussian behavior, which are known to occur when the experimental errors are predominantly systematic.)

Are the new data consistent with the previous experiments? can be addressed by observing the increase in χ^2 for the original data that occurs when the fit is adjusted to accommodate the new data.

Are the new data sets consistent with each other? can be studied by observing the change in χ^2 for each new data set in response to changing the weights for the other new data sets. This will reveal whether two new data sets “pull” in the same direction, or whether on the contrary there is a “tension” between them; or whether they measure different features, and so have little effect on each other.

Do the new data sets provide significant new constraints? can be studied in a simple way by exploring the range of acceptable fits to the original data using the Hessian (eigenvector) method, and observing how many of these eigenvector sets produce acceptable fits to the new data.

CDF _I N=33		D0 _I N=90		CDF _{II} N=72		D0 _{II} N=110		$\Delta\chi^2$ nonjet
Wt	χ^2	Wt	χ^2	Wt	χ^2	Wt	χ^2	
0	55.4	0	115.3	0	99.5	0	134.0	0.0
1	52.6	1	47.0	0	105.6	0	138.3	11.8
0	56.6	0	82.2	1	85.6	1	124.1	6.2
1	52.1	1	59.4	1	88.5	1	121.5	9.6
0	58.4	0	60.9	10	79.6	10	120.4	39.9
1	54.8	1	58.8	10	80.3	10	120.0	39.4
10	54.1	10	35.6	0	112.9	0	156.7	24.1
10	53.1	10	38.6	1	102.6	1	142.3	21.9
10	51.6	10	49.7	10	82.8	10	120.9	39.6
10	49.5	0	73.5	0	110.4	0	125.3	12.5
0	58.6	10	32.1	0	122.7	0	172.2	25.2
1	59.6	1	67.5	10	75.2	1	130.9	32.0
1	50.6	1	60.0	1	93.0	10	116.5	20.6
50	47.3	0	74.0	0	123.9	0	139.3	80.5
0	66.8	50	30.6	0	140.0	0	189.1	58.6
1	63.4	1	70.4	50	71.6	1	140.0	92.9
1	50.5	1	61.6	1	96.6	50	112.6	113.8

TABLE I: χ^2 for jet experiments with various weights

We will carry out these studies explicitly for the case of the four inclusive jet data sets from the Tevatron: CDF Run I, D0 Run I, CDF Run II, D0 Run II. Of these, only the Run I sets were included in the CTEQ6–CTEQ6.6 analyses. It is well known that the Run I data had a substantial impact on the determination of the gluon distribution at large x . It will be interesting to see whether the Run II data, which are based on a much larger integrated luminosity, provide significant new constraints. It will also be interesting to see whether the Run I data still play a significant role after the higher-statistics Run II data have been included. It will further be interesting to see whether the data from Run II pull the fit in the same directions as Run I, or if there is tension between the implications of the old and new data sets. We can similarly ask about possible tension between the CDF and D0 data sets. These are questions that have been raised at a number of workshops, but they have not been approached with the methods we describe here.

The information needed to answer these questions is contained in Table I, which shows χ^2 for each of the

4 jet experiments obtained by minimizing the total weighted χ^2 under a variety of choices for the weights assigned to those experiments. The weighted χ^2 for the sum of all nonjet experiments is shown in the last column, with the no-jets best fit value subtracted for convenience.

The question of whether the jet data sets agree with theory according to the “hypothesis testing” criterion is answered by seeing whether the χ^2 for these sets lie within the expected statistical range $N \pm \sqrt{2N}$, where N is the number of data points in the experiment.

1. For CDF_I, the expected range is 25–41. The fit with all jet weights 1 lies a little outside that range. This appears to result from unusually large fluctuations in a couple of the data points: these data cannot be fitted at much better χ^2 using *any* plausible smooth function, as is evidenced by the fact that χ^2 drops to only 47 when a weight of 50 is assigned to this experiment. (The purpose of including fits with a such a large weight in Table I is exactly to obtain this kind of information.) Unlike the other jet experiments, CDF_I has data only in the central rapidity region. It is therefore less sensitive to the gluon distribution than the others—in spite of its historic importance in changing the view of the gluon at large x ! The range of χ^2 for this experiment over the entire series of fits shown in the table is quite small, and it therefore has rather little influence on the contemporary global fit.
2. For D0_I, the expected range is 77–103. The best-fit χ^2 in the fit with all jet weights equal to 1 is 59, dropping to 32 at weight 10 for this experiment. If only the Run I data with weight 1 are included, we obtain $\chi^2 = 47$ with the new gluon parametrization, 68 for CTEQ6.5M, 99 for CTEQ6.6M, 124 and 138 for restricted gluon parametrizations shown in Tables 2 and 3. Thus this experiment is certainly consistent with the theory, although the unexpectedly large range of variations in χ^2 (despite the similarity in the explored PDF parametrizations) is suggestive of pronounced non-Gaussian behavior of the systematic errors for this data set. The fact that fits to these data can be obtained with χ^2 so much smaller than the number of points also suggests that there is something peculiar about the errors. (The correlated systematic errors for this experiment were published only as a single covariance matrix, rather than being broken out as individual shifts associated with each specific source of systematic error, whose magnitudes can be directly examined for plausibility.

Systematic errors given in this form could nevertheless be analyzed using principal component analysis [18], but we have not yet carried this out.)

3. For CDF_{II} , the expected range is 60–84. The fit gives $\chi^2 = 88$ with all jet weights equal to 1, dropping to 75 for weight 10; which implies that these data are consistent with theory.
4. For D0_{II} , the expected range is 95–125. The fit gives $\chi^2 = 121$ with all jet weights equal to 1, dropping to 116 for weight 10; again eminently consistent with theory.

The question of whether the jet data sets are consistent with the rest of the data in the global analysis can be addressed by observing the increase in χ^2 for the nonjet data that occurs when the fit is adjusted to accommodate the jet data. Table I shows that χ^2 for the nonjet data is forced to increase by only 9.6 to accommodate the 4 jet experiments at weight 1, and only by 39.6 to accommodate them at weight 10. In our previous studies of these data for CTEQ6.6, we estimated that an increase of $\Delta\chi^2 = 100$ could be tolerated at the 90% confidence level, so the jet experiments appear consistent with the nonjet data. Note that we take the “hypothesis testing” point of view of requiring that χ^2/N be acceptable for all of the experiments, rather than the more stringent “parameter fitting” ($\Delta\chi^2 = 1$) point of view for estimating the uncertainty limits [17].

The question of whether the four inclusive jet experiments are consistent with each other in the fit can be studied by looking at how increasing the weight for some of them affects the χ^2 for the others. From Table I, we observe the following:

- *The two Run II experiments are fairly consistent with each other*, since for example when CDF_{II} is assigned weight 10, its χ^2 is not strongly dependent on whether D0_{II} is assigned weight 1 or 10; and similarly when D0_{II} is assigned weight 10, its χ^2 is not strongly dependent on whether CDF_{II} is assigned weight 1 or 10. However, in each case there is a small increase in χ^2 for one of the experiments when the weight for the other is increased, which suggests a bit of tension between them. That is in fact the case, as can be seen clearly using a new and more powerful method of analysis that is discussed in a separate publication [19].
- *The consistency between Run I and Run II measurements is ambiguous*. If the Run II experiments are assigned weight 10, then raising the weight for Run I data from 1 to 10 improves the fits to Run I as it must, while making very little change in the χ^2 for the Run II and nonjet experiments. This suggests that Run I and

Run II data are rather compatible with one another. On the other hand, if instead the Run I experiments are assigned weight 10, then raising the weight for Run II data from 1 to 10 (which improves the fits to Run II dramatically) raises χ^2 for D0_{I} from 38.6 to 49.7. An increase of this magnitude suggests tension between Run I and Run II—and, indeed, the Run I and Run II experiments prefer somewhat different shapes of the gluon PDF, as will be shown in Sec. 7. Yet the statistical significance of this level of disagreement cannot be established firmly, given the abnormally large variations in χ^2 for D0_{I} that are observed for otherwise very similar fits. This may be related to the same details of the systematic error treatment in D0_{I} that allows χ^2/N to become very small for that experiment. We keep the Run I data in our final global fit. The fact that the Run I and Run II experiments are at somewhat different \sqrt{s} values (1.80 TeV vs. 1.96 TeV) might possibly supply some useful physics constraint. Also, D0_{I} extends to higher rapidity than either of the Run II data sets. The effect of this choice will be studied in Sec. 7 by examining the effect of instead dropping the Run I data.

Finally, let us address the question of whether the Run II jet data can be expected to reduce the PDF uncertainty. Table I shows that the fit with weight 1 for both Run I experiments and weight 0 for both Run II experiments has $\chi^2 = 106$ and 138 for the two Run II experiments. Trying each of the 44 eigenvector uncertainty sets of CTEQ6.6, we obtain extreme χ^2 values of 119 for CDF_{II} and 140 for D0_{II} . None of these values indicate a drastically bad fit, so no great reduction in the PDF uncertainty can result from including the new jet data. However, some of the values both for CDF_{II} and D0_{II} are sufficiently larger than the values shown in Table I, that *we can expect a small reduction in the PDF uncertainty as a result of including the new data*. That reduction in uncertainty is examined directly in Sec. 6.1.

5.1. Fits with restricted gluon parametrizations

As discussed in Sec. 4, it is important to use a sufficiently flexible parametrization for the input gluon distribution. The following studies demonstrate how an inadequate parametrization can be exposed by the weighting method.

If we restrict the parametrization (1) by setting $a_4 = a_5 = 0$, we obtain the results shown in Table II. With that restriction, the fit to data without jets is still very good: χ^2 is higher by only 2 units. But the fit to these nonjet data becomes very bad when the jet

weights are raised to 10 or more; while for smaller jet weights, the fits to the jet experiments are much worse than the corresponding fits of Table I. If this simplified parametrization had been used, the jet data would have mistakenly appeared to be inconsistent with the rest of the data.

CDF _I N=33		D0 _I N=90		CDF _{II} N=72		D0 _{II} N=110		$\Delta\chi^2$ nonjet
Wt	χ^2	Wt	χ^2	Wt	χ^2	Wt	χ^2	
0	55.8	0	145.9	0	120.6	0	155.2	2.0
1	53.2	1	124.0	0	118.2	0	148.6	7.7
0	58.6	0	121.3	1	98.1	1	137.8	16.8
1	54.5	1	108.8	1	95.5	1	134.2	25.8
10	54.1	10	75.7	0	142.0	0	152.1	184.3
10	51.9	10	74.0	1	101.6	1	134.6	185.5
0	67.1	0	75.3	10	77.3	10	126.1	114.6
1	60.3	1	74.1	10	77.1	10	125.8	119.3
10	51.7	10	64.5	10	76.2	10	126.1	204.3

TABLE II: Fits to jet experiments with various weights, using a restricted gluon parametrization.

A different simplified gluon parametrization

$$g(x) = a_0 x^{a_1} (1-x)^{a_2} (1 + a_3 x), \quad (2)$$

which has been used in studies at HERA [20] (at a somewhat higher μ_0), has even worse behavior, as is shown in Table III. For here, χ^2 for the nonjet data rises by 91.4 when the jet data are included at weight 1; and that weight is not even large enough to obtain good fits to the jet data. It is perhaps not surprising that the form (2) is inadequate, because the coefficient a_0 of the leading behavior x^{a_1} at $x \rightarrow 0$ and the coefficient $a_0(1 + a_3)$ of the leading behavior $(1-x)^{a_2}$ at $x \rightarrow 1$ might have very different magnitudes, since those limits are governed by unrelated physics. Hence the limiting behaviors might require $1 + a_3$ to be very large or very small, in which case the linear approximation $1 + a_3 x$ provided by Eq. (2) would have to cover a large range of variation, for which it might be a worse approximation than the exponential form in (1).

6. UNCERTAINTY OF THE GLUON DISTRIBUTION: COMPARISON OF METHODS

In this section, we discuss various methods to determine the uncertainty of parton distributions. We focus on the gluon distribution at large x because that is the primary aspect of the global analysis that is influenced by the jet experiments. Because the uncertainty in the

CDF _I N=33		D0 _I N=90		CDF _{II} N=72		D0 _{II} N=110		$\Delta\chi^2$ nonjet
Wt	χ^2	Wt	χ^2	Wt	χ^2	Wt	χ^2	
0	57.8	0	175.4	0	139.5	0	180.9	4.3
1	54.5	1	137.9	0	148.5	0	165.8	91.4
0	64.0	0	143.7	1	102.4	1	151.4	27.8
1	53.9	1	128.4	1	105.4	1	143.0	110.7
10	56.3	10	74.2	0	174.7	0	166.2	235.1
10	53.5	10	75.6	1	115.8	1	139.6	299.2
0	79.3	0	79.0	10	75.8	10	131.8	156.9
1	68.5	1	77.8	10	75.2	10	131.7	163.9
10	54.4	10	67.7	10	72.8	10	131.8	259.0

TABLE III: χ^2 for jet experiments with various weights, using the restricted gluon parametrization (2).

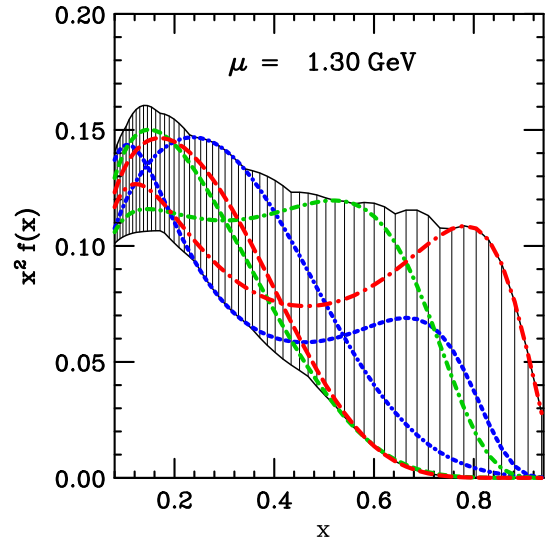


FIG. 3: Gluon uncertainty range by LM method, and some of the specific fits that define the limits.

gluon is large, it serves as a strong test of the methods used to estimate uncertainties.

Within the usual context of our global analysis [4], parton distribution shape parameters that minimize an effective weighted χ^2 function define the “best fit”. All parton distributions defined by the other choices of the parameters are deemed acceptable (and delineate the region of the PDF uncertainty allowed by the analysis) if they produce a value of χ^2 that exceeds the minimum value by no more than a given tolerance value $\Delta\chi^2$ (i.e., $\chi^2 \leq \min(\chi^2) + \Delta\chi^2$). Appropriate weights and the tolerance criterion must be chosen to ensure that all of the accepted fits provide adequate descriptions of every data set. In the present case, we

estimate that $\Delta\chi^2 = 100$ provides an approximately 90% confidence limit for all experiments included in the fit.

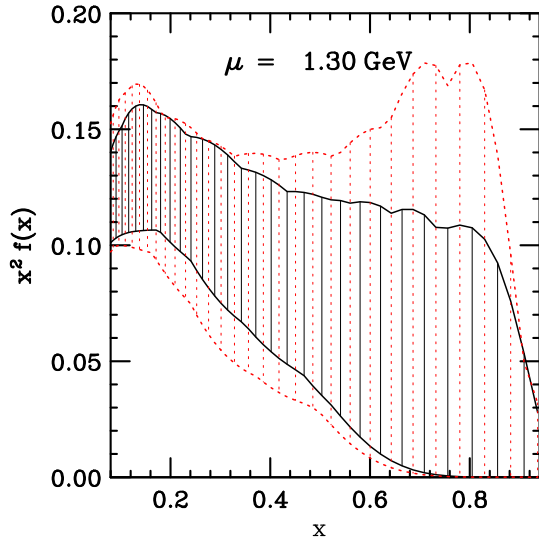


FIG. 4: Gluon uncertainty range by LM method: smaller region same as in Fig. 3; larger region = without Run II jet data.

6.1. Lagrange Multiplier method

The uncertainty of the gluon distribution can be found in a straightforward way by the Lagrange Multiplier (LM) method [21]: at any given value of x , a term $\lambda g(x, \mu_0)$ is added to the χ^2 function that is minimized by varying the fitting parameters. The parameter λ is adjusted to make the increase in χ^2 above its minimum value equal to $\Delta\chi^2$. This yields two allowed PDF sets (one from positive λ and one from negative) that provide the minimum and maximum $g(x, \mu_0)$. The procedure is carried out at a number of x values to map out the extremes of the uncertainty range.

Results for the gluon uncertainty obtained in this way are shown in Fig. 3, together with some of the specific curves that produced the envelope of extremes. The shapes that provide the extremes do not violate any strong intuition, although those showing a peaked structure in $x^2 g(x, \mu_0)$ at large x might not be expected *a priori*. (Still larger uncertainties might be found if more fine structure were allowed by the parametrization; but sharp structures in x are not physically expected, and their effect would tend to go away at higher scales through the smoothing character of DGLAP evolution.)

It is natural to ask if the extensive new jet data from Run II reduce the gluon uncertainty. To answer that question, Fig. 4 compares the uncertainty range from Fig. 3 with the uncertainty range obtained by a similar Lagrange Multiplier calculation with the Run II data removed from the fit. *One sees that the Run II data somewhat reduce the gluon uncertainty at large x .*

6.2. Quartic penalties

A PDF set that deviates from the minimum χ^2 by an amount $\Delta\chi^2 = 100$ usually provides an acceptable fit to all experiments and thus cannot be ruled out as a valid possibility within the uncertainty range according to the conservative “hypothesis testing” criterion. But if the increase in χ^2 is not spread widely over the ~ 3000 data points, but rather is concentrated in one or two experiments, or in any small subset of the data points, it may be an unacceptable fit. This is found to happen for some of the extreme gluon distributions obtained in Sec. 6.1, because only the inclusive jet experiments are sensitive to the gluon distribution at large x .

To avoid this problem, we could increase the weight for the jet experiments in the total χ^2 by trial and error. But we find it simpler and more effective to add a penalty to χ^2 that is proportional to $(\chi^2/N)^4$ for each of the jet experiments, in order to force the final fit to agree acceptably with each of those experiments, without introducing much change in the central fit. With this change in the definition of the weighted χ^2 that is minimized, we can continue to use our established calculational tools. (An alternative method used by MSTW [6] is to abandon a fixed $\Delta\chi^2$ and instead to set the maximum allowed displacement along each eigenvector direction independently, by monitoring the quality of fit to each of the data sets along that direction.) The quartic form for the penalty adds little to χ^2 except near the boundary, so it does not significantly alter our $\Delta\chi^2 = 100$ tolerance estimate.

These “quartic penalties” are included in all subsequent fits in this paper. Our final uncertainty for the gluon distribution is therefore appreciably smaller than what is shown in the preliminary study of Figs. 3 and 4.

6.3. Hessian eigenvector method

In addition to the LM method, the other standard technique for estimating PDF uncertainties is the Hes-

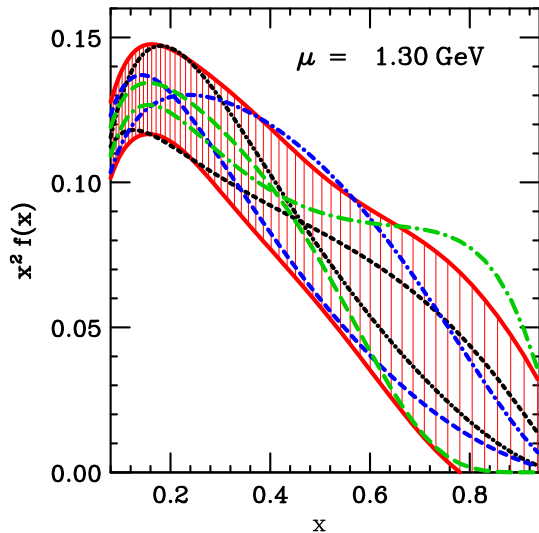


FIG. 5: Gluon uncertainty by Hessian method, compared to extremes at $x = 0.20, 0.55, 0.80$ by LM method.

sian eigenvector method [22]. That method works as follows. The first derivatives of χ^2 with respect to the fitting parameters are zero at the minimum, so in the neighborhood of the minimum, χ^2 can be approximated by Taylor series as a quadratic form in the fitting parameters. The coefficients of that quadratic form are the Hessian matrix, which is the matrix of second derivatives of χ^2 with respect to the fitting parameters. The eigenvectors of the Hessian matrix can be used to define eigenvector PDF sets that characterize the allowed uncertainty range. The uncertainty of any prediction is calculated by computing the deviation from the best fit along each eigenvector direction, and adding those deviations in quadrature separately for the positive and negative deviations. The gluon uncertainty calculated this way is shown in Fig. 5, together with extremes calculated by LM at $x = 0.2, 0.5$, and 0.8 . The agreement between the two methods is seen to be quite good, although a slightly larger upper limit is found at $x = 0.8$ by the LM method, which is not subject to the quadratic approximation. The eigenvector method is of course much more convenient to use than LM, because the LM method requires tuned fittings of the Lagrange Multiplier parameter for every extremum point that is desired. So it is comfortable to see this agreement.

6.4. Choice of eigenvectors

The eigenvectors of the Hessian matrix can be thought of as a choice of basis vectors that define new fitting parameters z_i for which

$$\chi^2 = \chi_{\min}^2 + \sum_{i=1}^N z_i^2 + \mathcal{O}(z^3). \quad (3)$$

The choice of these eigenvectors is not unique, because the form (3) is preserved by any further orthogonal transformation of the coordinates $\{z_i\}$. In the approximation that χ^2 is a quadratic function of the shape parameters which parametrize PDFs at μ_0 , such a transformation would not affect the calculation of the uncertainty.

The freedom to make an additional orthogonal transformation may offer the possibility to reduce the number of eigenvectors that are needed to effectively describe the uncertainty of a particular quantity of interest. One possible way to attempt this is to diagonalize the parameter dependence of that quantity, using a procedure that is sketched in the Appendix and described explicitly in [19].

An example of this is shown in Fig. 6, which shows the gluon uncertainty calculated by the eigenvector method, together with the 48 extreme eigenvector sets (positive and negative directions along each of the 24 eigenvectors). In the left panel, the eigenvectors are defined in the traditional way as eigenvectors of the Hessian. Note that many eigenvectors contribute to the uncertainty at each value of x . (A common method to make a quick estimate of uncertainty is simply to look at the extremes over the eigenvector sets, without adding the individual contributions in quadrature. That can easily underestimate the uncertainty by a factor of two or more, as seen here.)

In the right panel of Fig. 6, the eigenvectors are defined by choosing $G = g(0.55, \mu_0)$ in Eq. (A3) of the Appendix. Note that close to $x = 0.55$, almost all of the uncertainty comes from just one pair of eigenvector sets. In CTEQ6.1, it happened by convenient accident that most of the uncertainty in the gluon distribution was embodied in a single eigenvector set. By “redialyzing” the Hessian matrix, this type of simplicity can be gained in other situations; though as seen in Fig. 6 it may take more than one eigenvector direction to span the important variations.

A redialyzation based on the second-derivative matrix, such as the one carried out here, is not necessarily the best way to choose the new eigenvector directions, since there is no theorem to guarantee that it will result in only a few dominant coefficients. For

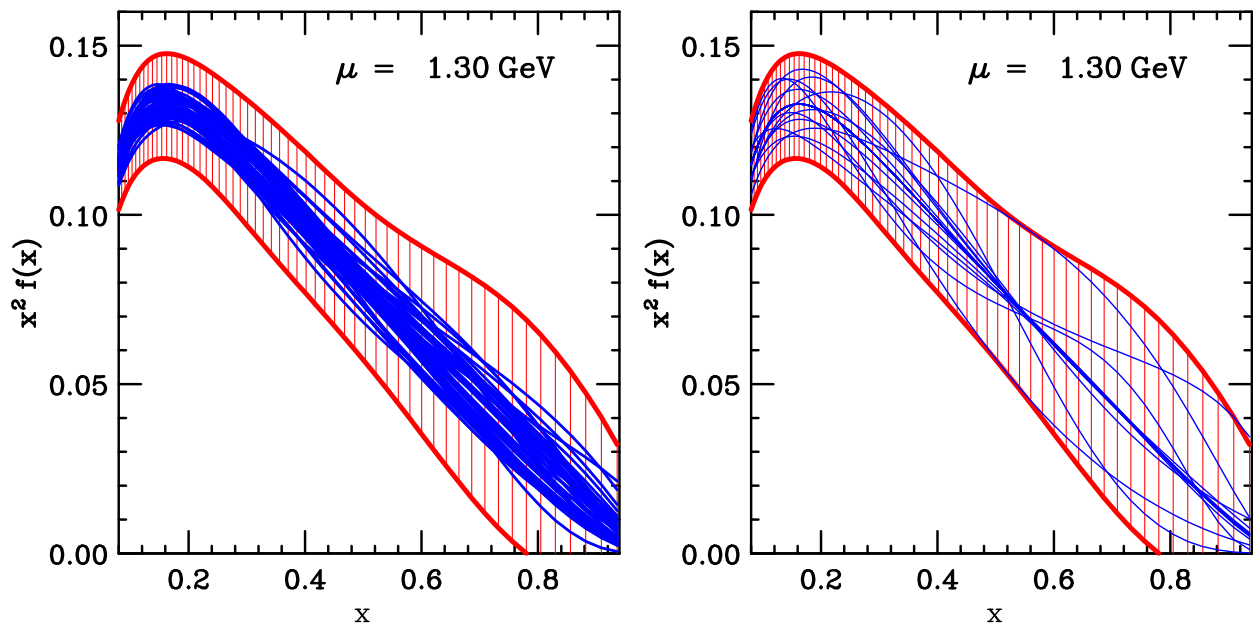


FIG. 6: Gluon distributions and uncertainties in CT09 (red) and the eigenvector contributions to them. Left: eigenvectors by traditional method; Right, eigenvectors by “rediagonalization” method based on diagonalizing $g(\mu_0, x)$ at $x = 0.55$.

example in this particular case it might have worked better to ignore the second derivatives, and instead to simply choose the first new eigenvector direction along the gradient direction for, say $g(0.5)$ in the 24-dimensional space; then the second eigenvector could be chosen along the gradient direction for, say $g(0.8)$ in the 23-dimensional subspace that is orthogonal to the first eigenvector, etc. In any case, the option of redefining the eigenvector directions to simplify the description of uncertainties in other physics analyses shows promise for further study.

6.5. Random PDF sets

Another possible way to characterize the uncertainties would be to generate a random collection of PDF sets that lie inside or at the edge of the acceptable range $\chi^2 \leq \chi_{\min}^2 + \Delta\chi^2$. (In the quadratic approximation, this would correspond to a sphere in the N -dimensional hyperspace spanned by $\{z_i\}$.) For example, a set at the edge can be constructed by generating a random unit vector in the N -dimensional parameter space using the eigenvectors as basis vectors, and moving away from the minimum point in that direction until χ^2 has increased by the tolerance $\Delta\chi^2$. The envelope of results obtained from 500 PDF sets obtained this way is shown in Fig. 7, together with 50 of

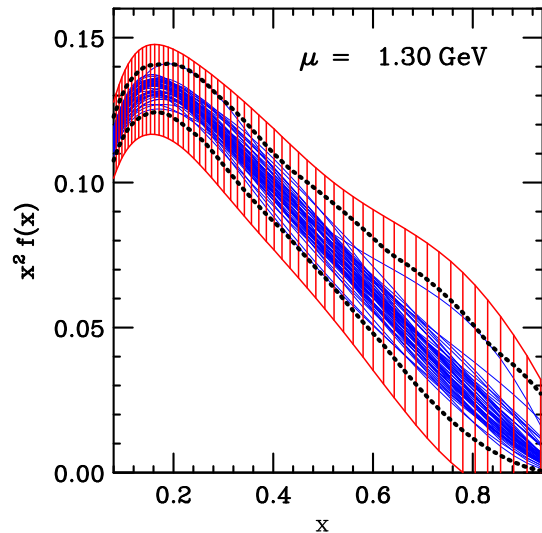


FIG. 7: Gluon uncertainty from 50 random PDF sets with $\Delta\chi^2 = 100$; envelope of 500 such random sets (dotted); full uncertainty range from Hessian method (shaded region).

the individual results. Also shown is the uncertainty obtained by the Hessian method. *We see that the envelope of the random sets covers a much smaller range than the full uncertainty—even though every one of the 500 sets is at the upper limit for χ^2 .* This is not sur-

prising, since the extreme $g(x)$ at any given x can be thought of as corresponding to a specific direction in the N -dimensional parameter space. The probability distribution for the component, z , of a random unit vector along any particular direction in N dimensions can be shown to be $dP/dz \propto (1 - z^2)^{(N-3)/2}$, which becomes extremely small as z approaches its limit of 1. For example, when $N = 24$, the probability for $z > 0.6$ is less than 1 in 1000, so the chance of finding a value close to the true extreme of 1.0 by random sampling is very small. This conclusion can be understood qualitatively in a simple way: it is unlikely for the direction cosine along any particular direction to lie close to its maximum of 1, since there are N random direction cosines whose sum of squares must add up to 1.

The point of this exercise is to show that no conveniently small collection of PDFs that are all acceptable fits to the data can approximately cover the full uncertainty range. It is therefore essential to have a well-defined way to combine the uncertainties associated with the various fits in such a collection. In the Hessian method, this is provided by the rule of adding uncertainties from eigenvector sets in quadrature. In the case of random PDF sets, it would require estimating the uncertainty range for a prediction of a quantity X using the dispersion $\langle X^2 \rangle - \langle X \rangle^2$ in values calculated from the random sets.

The above limitation does not apply to Monte Carlo based sampling methods such as NNPDF [16], since those methods produce a collection of PDF sets that directly samples the space of uncertainties. Such a collection naturally includes some PDF sets that are not “acceptable” fits to the input data—e.g., in a collection of 100 Monte Carlo sets, one obviously expects to find ~ 10 sets that lie outside of the 90% confidence region. In this approach, the PDF uncertainty for a quantity is obtained by simply calculating that quantity for each of the sample PDF sets: the distribution of results directly represents the predicted uncertainty range.

7. UNCERTAINTY OF THE GLUON DISTRIBUTION: RESULTS

The CT09 fit discussed in Secs. 6.3 and 6.4 is our most up-to-date set of parton distributions. The central gluon fit and its uncertainty are shown in Fig. 8 at scales $\mu = 2 \text{ GeV}$ and 100 GeV , compared with the previous CTEQ6.6 [5] fit. The uncertainty band has narrowed somewhat as a result of including the new jet data and the quartic penalties—except at extremely large x , where the more flexible gluon parametrization

in CT09 has broadened the allowed range. There is a strong overlap between the old and new uncertainty bands, and the central fit has shifted by an amount that is within or just at the edge of those bands. At a large scale such as $\mu = 100 \text{ GeV}$, there is rather little change between the old and new determinations.

Fig. 8 shows that the CT09 central fit at small scale has a featureless behavior at large x , in contrast to the mild “shoulder” structure of CTEQ6.6. (The appearance of this shoulder is enhanced by the factor x^2 that multiplies $g(x)$ in the plot to emphasize the large x behavior.) Indeed, MSTW [6] remark that in fitting the new jet data, they no longer need to use their former convoluted method of parametrizing the gluon in the DIS scheme and transforming it to $\overline{\text{MS}}$. However, we find that with a properly flexible parametrization, some type of shoulder structure is not ruled out—indeed, the original CTEQ6.6 central fit for the gluon distribution still lies within our allowed uncertainty range. In detail, χ^2 for the jet experiments (CDF_I, D0_I, CDF_{II}, D0_{II}) are (54, 59, 91, 122) in CT09; (52, 55, 116, 121) in a fit with the gluon shape identical to CTEQ6.6; and (53, 60, 97, 120) in a fit using the CTEQ6.6 gluon parametrization with the parameters refitted.

The change between CTEQ6.6 and CT09 in the shape of the gluon distribution is a consequence of interplay between adding the Run II jet data and increasing the flexibility of the gluon parametrization. This is studied in Fig. 9. The solid curve and shaded region are again CT09 and its uncertainty. The dotted curve is CTEQ6.6. The dot-dash curve is the result of repeating the CTEQ6.6 fit using the CT09 gluon parametrization. Note that this increased freedom for the gluon shape enhances the shoulder, and does not move the fit closer to CT09. The short-dashed curve is the result of including the Run II data, with all other details of the fit being the same as in CTEQ6.6: this changes the fit about half way to CT09. But with the Run II data included, bringing in the more flexible gluon parametrization now produces the rest of the change to CT09. Finally, the long-dashed curve is a fit that is identical to CT09 except for dropping the Run I jet data. This answers the question raised earlier regarding the degree of tension between Run I and Run II jet data from a practical point of view: we see that the effect of the Run I data on the fit is noticeable but small compared to the other uncertainties.

It is instructive to examine the preferences of various combinations of the four jet data sets in the fit. This is shown in Fig. 10. The solid curve and shaded region are again CT09 in both panels. The other curves were obtained by fits with weight 1 for all nonjet experiments, and weights 0 or 1 for each jet experiment

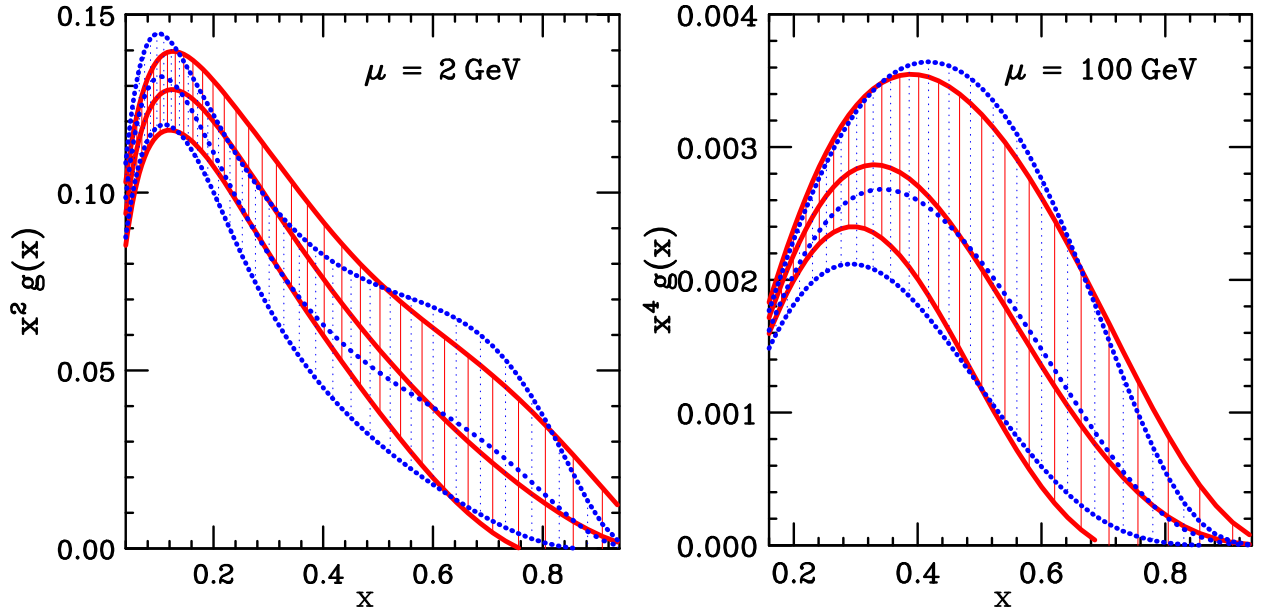


FIG. 8: Gluon distributions and uncertainties in CT09 (solid) and CTEQ6.6 (dotted). A stronger weight factor x^4 is used in the right-hand panel ($\mu = 100$ GeV) to accentuate the large- x behavior.

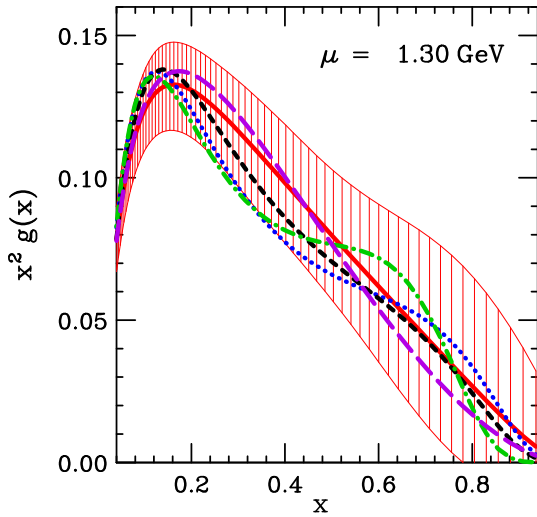


FIG. 9: CT09 and variations (see text).

as listed in the captions. The four curves in the left panel correspond to the first four fits in Table I. There is a slight difference between the (1,1,1,1) curve and CT09, because we have chosen to apply somewhat larger weights (1.3,1.3,2.1,2.1) to these experiments in CT09. The fit with no input from jet data (0,0,0,0) is substantially lower than any of the other fits at large

x —this is a review of why the first jet data made such a strong impact on the gluon determination! The four curves in the right panel show the preferences of the individual jet experiments. The D0_I data shows its famous preference for a peak at large x ; though Table I shows that it can be fit with nearly as good χ^2 without the peak. The difference between the CDF_{II} and D0_{II} curves is comparable to our error estimate, which affirms that our error estimate is not overly conservative.

Figure 11 explores the consequences of some of the choices that were made in producing CT09. The solid curve and shaded region are CT09 itself at scale 2 GeV. We first change the quark masses $m_c = 1.3 \rightarrow 1.4$ GeV and $m_b = 4.5 \rightarrow 4.75$ GeV, and change $\mu_0 = 1.3 \rightarrow 1.4$ GeV to maintain $\mu_0 = m_c$. These changes are found to have a negligible effect on the gluon distribution: the change is smaller than the width of the line in the figure.

In our basic fitting procedure [4] we routinely employ weight factors to improve the quality of fit to certain key experiments. In particular, weights of 1.3 and 2.1 were applied to the Run I and Run II data respectively in CT09, and a further contribution proportional to $(\chi^2/N)^4$ was added for these experiments as discussed in Sec. 6.2. The dotted curve in Fig. 11 shows the effect of setting all of the weight factors to 1 (including those for the jet experiments) and dropping

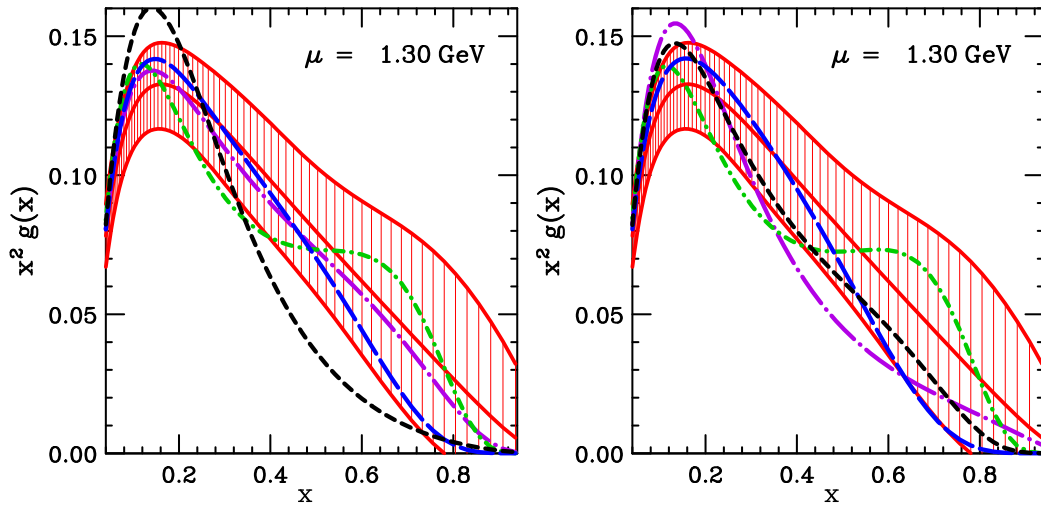


FIG. 10: Fits with various weights (CDF_I , $D0_I$, CDF_{II} , $D0_{II}$). Left panel: Long dashed dotted = (1,1,1,1), Short dashed dotted = (1,1,0,0), Long dashed = (0,0,1,1), Short dashed = (0,0,0,0). Right panel: Long dashed dotted = (1,0,0,0), Short dashed dotted = (0,1,0,0), Long dashed = (0,0,1,0), Short dashed = (0,0,0,1).

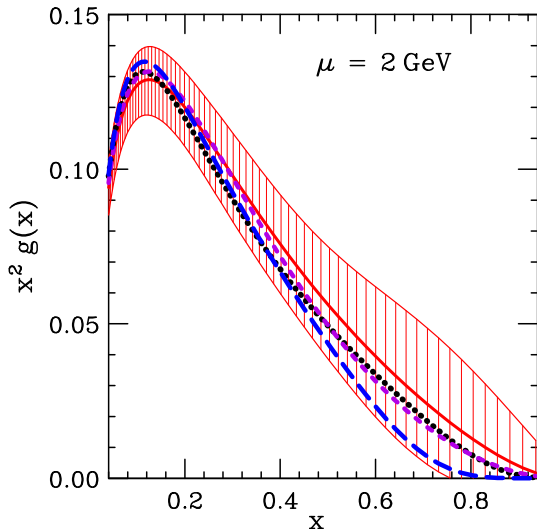


FIG. 11: CT09 and results from some alternative choices (see text).

the quartic penalty. The resulting change is very small. (The real purpose of the weights is toward maintaining acceptable fits to all experiments as we move away from the best fit to estimate uncertainties.)

The short-dash curve in Fig. 11 shows the effect of dropping the Run I data, keeping the weights at 1, but restoring the quartic penalties on Run II jet χ^2 values. Finally, the long-dash curve is similar except that the

quartic penalties have also been dropped. This fit has weight 1 for all experiments except for dropping the older jet data, and no extra penalties added to χ^2 . Some would argue this to be the most natural choice; though our belief is that it is preferable to apply some emphasis in the global fit to experiments that measure an important feature with a relatively small number of data points. In any case, the uncertainty band shown is seen to do a reasonable job of encompassing the results of various plausible choices. If it were made much narrower by a smaller $\Delta\chi^2$ criterion, it would not do so. *Thus we see that a large part of the uncertainty—and the need for the $\Delta\chi^2 \sim 100$ criterion—arises from differences in plausible choices involved in making the global fit, rather than directly from propagating the experimental errors given in the data.*

8. COMPARISON WITH MSTW

We compare our work with recent results from MSTW [6] in Fig. 12. The solid curve and shaded region show the central fit and uncertainty range for CT09, as in the preceding figures. To make a straightforward comparison, all other curves in Fig. 12 use the MSTW values $\alpha_s(m_Z) = 0.12018$, $m_c = 1.4$ GeV, $m_b = 4.75$ GeV. The dotted long dashed curve is a fit that is the same as CT09 except for the change in $\alpha_s(m_Z)$ (and the change in quark masses, which has a negligible effect).

The dotted short dashed curve is MSTW2008NLO.

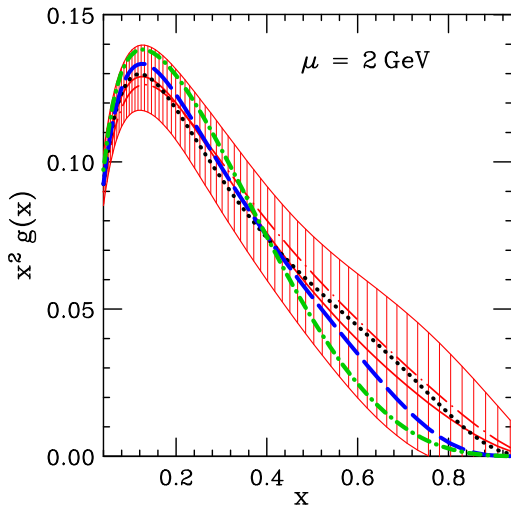


FIG. 12: Solid curve and shaded region is CT09 ($\alpha_s(m_Z) = 0.118$). All other curves are fits with $\alpha_s(m_Z) = 0.12018$. Dotted short dashed curve is MSTW2008NLO. See text for description of the other curves.

It is surprisingly different from the α_s -modified CT09, though it lies within our estimated 90% confidence region.

To look for the cause of the difference between the α_s -modified CT09 result and MSTW, we explore a series of modifications to the CT09 procedure that make it more like that of MSTW. These are the same modifications that were discussed in connection with Fig. 11. First we drop the CDF_I and $D0_I$ data sets. This leads to the dotted curve in Fig. 12, which is closer to the MSTW result at large x , but still quite far from it.

The dashed curve in Fig. 12 corresponds to again dropping the Run I data sets, while also setting the weight factors for all experiments to 1 and dropping the quartic penalties on χ^2/N . This reduces the influence of the jet data, and hence results in a fit that is closer to no-jets fits, which have a lower gluon at large x . This dashed-curve fit is the most similar in its approach and result to that of MSTW; but a noticeable difference still remains. We can only speculate on what might be responsible for this difference, with obvious suspects being the different parametrizations used, or the neglect of correlated systematic errors for DIS data in the MSTW fit. Other possible sources for the difference is that there are some differences in which data sets are included in the fits, and a difference in the kinematical cuts in Q and W that are applied to those data sets. Furthermore, there are small differences in the treatment of heavy quarks; and a small

difference in the definition of $\alpha_s(\mu)$ at NLO, even when the values are matched at $\mu = m_Z$ (see [23, 24]).

9. QUALITY OF THE FITS

The good agreement of the central fits with the Run II jet data, when systematic error shifts allowed by the published data are included, is shown in Figs. 13 and 14. The unshifted data points are also shown. These are quite far from the theory curves: the systematic errors are much larger than the statistical ones here, so fitting the systematic error parameters is an essential part of fitting these data sets.

There are 24 systematic shifts for CDF_{II} , whose fitted values come out of order 1 as they should: -0.1, -1.0, -0.3, -1.0, 0.7, -0.2, 0.8, -0.7, -0.7, -0.9, 0.1, 0.6, 1.0, -0.3, -0.3, 0.5, -1.2, 0.4, 0.9, 0.0, -1.3, 0.1, -0.1, -0.3. The fitted overall normalization factor is 1.02, which is well within the published 6% error.

There are 22 systematic shifts for $D0_{II}$ (in addition to the overall normalization). Some of these come out a bit larger, though they are still of order 1: -0.5, -1.6, 0.0, 0.1, -0.8, -0.5, 0.1, 1.1, -0.4, 1.1, -1.1, -0.4, 0.4, -1.6, -0.2, -1.9, 0.5, 0.3, 0.2, 1.7, -1.1, -0.1. We presume these shifts to be reasonable, since their overall χ^2 probability is acceptable, and since—as is typical of systematic errors—their experimental assessment must be partly subjective. For what it is worth, we find it absolutely necessary for some of these shift parameters (most notably, “dsys015: eta-intercalibration fit”) to have magnitude larger than 1.5 in order to achieve an acceptable fit to these data within the global fit. The fitted overall normalization factor is 0.98, which is well within the published error estimate.

10. CONCLUSION

We have carefully examined the NLO treatment of inclusive jet data and its influence on the determination of the gluon distribution in a QCD global analysis. Key features of the analysis are the use of sufficiently flexible functional forms to reduce parametrization dependence, and full inclusion of the correlated systematic errors published by the experiments.

The difference between the new CT09 gluon results and our previous CTEQ6.6 analysis [5] is shown in Fig. 8. At a large scale like $\mu = 100$ GeV, where the high- x gluon PDF is important for many high-profile signal and background processes at the Tevatron and LHC, the impact of the new jet data is quite small com-

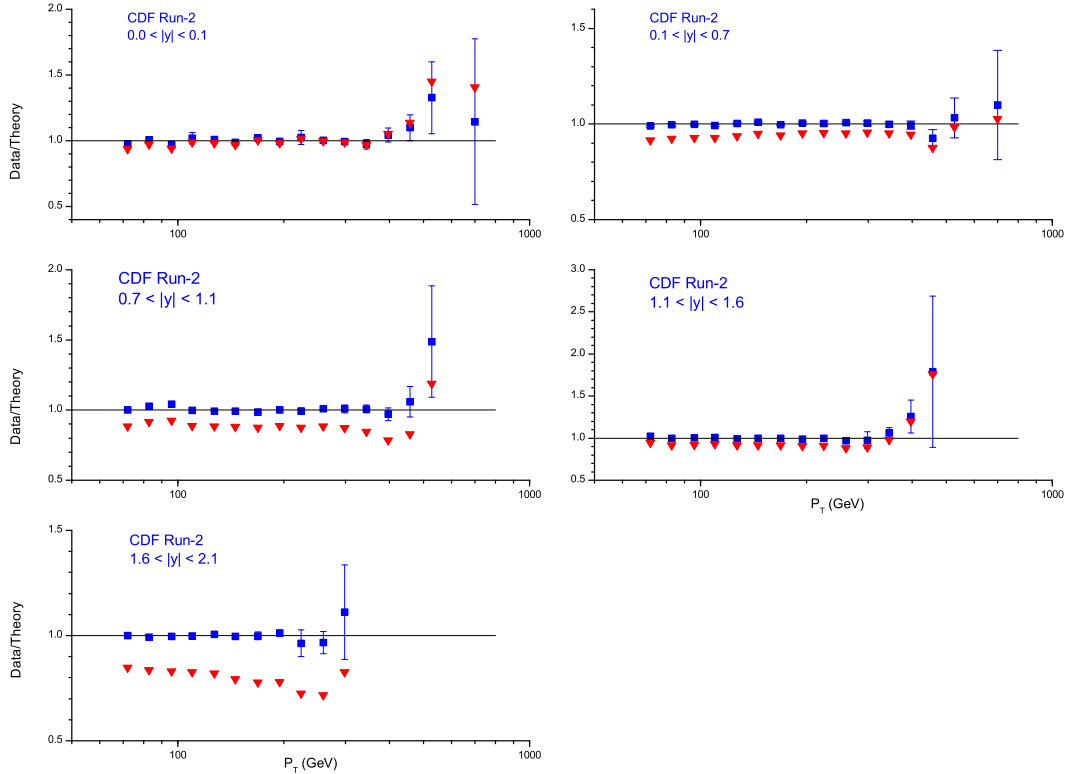


FIG. 13: Central fit to CDF Run II data. Triangles are the original data points. Squares with error bars include shifts due to the systematic errors, whose magnitudes are determined in the fit.

pared to the remaining uncertainty—as was expected from the outset, since the new data agreed fairly well with their prediction from CTEQ6.6 and its uncertainty range.

At the small scale $\mu = 2$ GeV, where the constraints on the gluon are rather indirect, Fig. 8 shows that the change in the central prediction at some values of x is close to the 90% confidence limit of the uncertainty estimated in CTEQ6.6. This demonstrates that our method does not overestimate those uncertainties, in spite of its tolerance for a range of χ^2 that is large by ideal statistical standards.

We have introduced an extension of the familiar Hessian matrix method [22] for uncertainty analysis. The extension involves making a further orthogonal transformation of the coordinates, after the transformation that diagonalizes the Hessian has been carried out. This leaves the Hessian matrix in its convenient diagonal form, while offering the possibility to describe the uncertainty on a given quantity using a small number of important eigenvector sets. This is illustrated in

the right-hand side of Fig. 6, where most of the gluon uncertainty near $x = 0.5$ is given by just one or two eigenvector pairs. A further application of this extension of the Hessian method provides a new and improved method to study the compatibility of the data sets in a global fit. This is described in a separate publication [19].

One value of this paper is to document and illustrate methods that can be used to incorporate new data sets into a global analysis. There will be many opportunities to apply this in the near future, as data from Tevatron Run II and HERA Run II continue to arrive, and with data from the LHC on the horizon.

To conclude with a speculation, it is interesting to compare the extracted gluon distribution with the distributions for up and down quarks. This comparison is shown in Fig. 15. The quark distributions have smaller uncertainties than the gluon—particularly the up quark, whose larger electric charge makes it prominent in the extensive body of neutral-current DIS measurements. Surprising as it may seem, we observe that

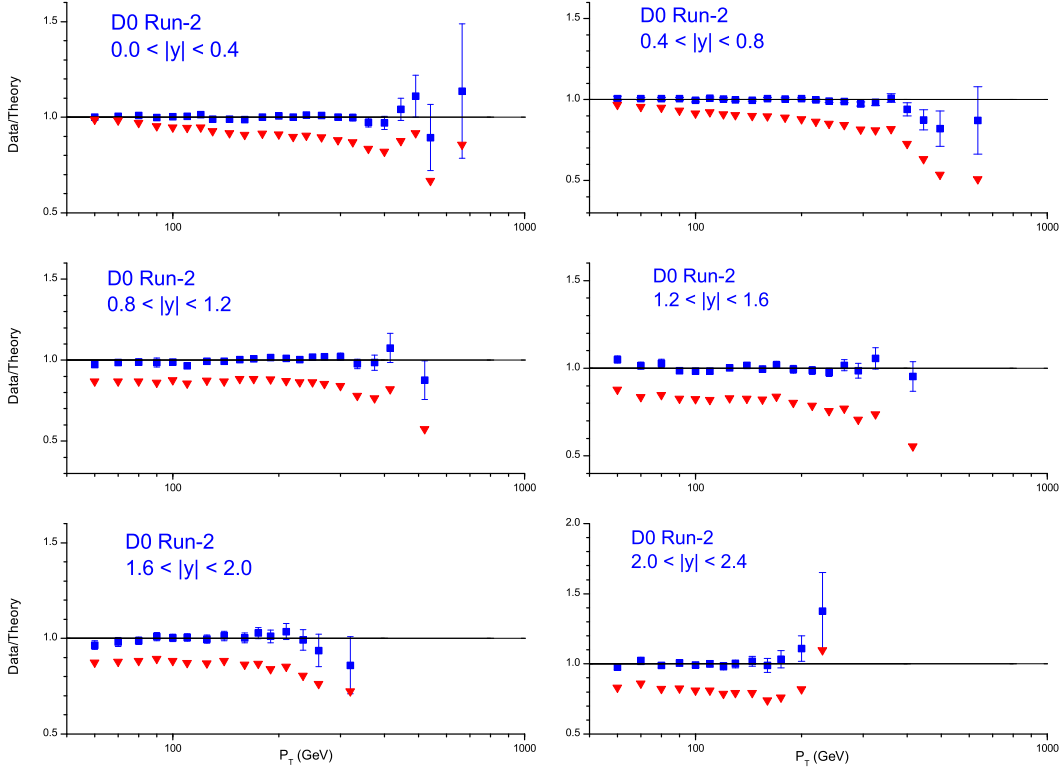


FIG. 14: Central fit to D0 Run II data. Triangles are the original data points. Squares with error bars include shifts due to the systematic errors, whose magnitudes are determined in the fit.

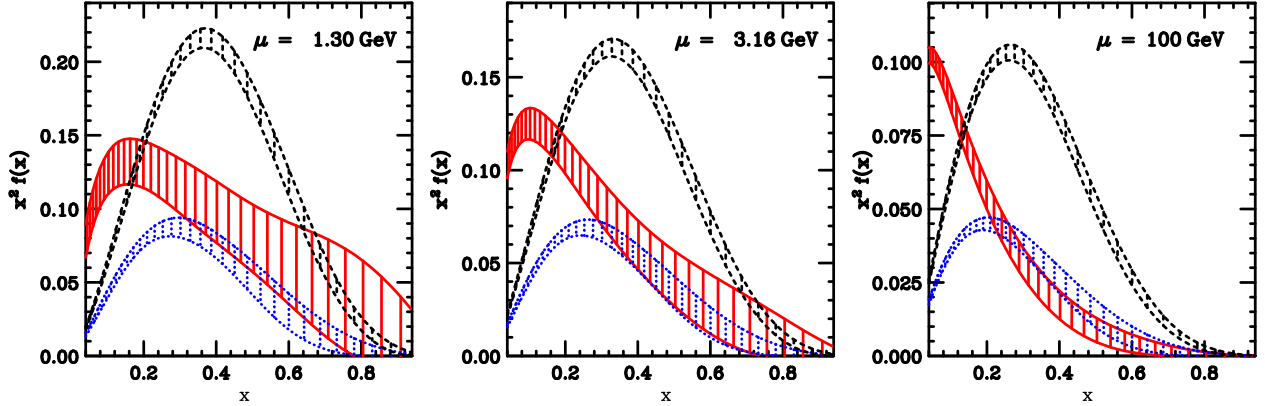


FIG. 15: Gluon (solid), u quark (dashed), and d quark (dotted) distributions at three different scales.

at a small scale like $\mu = 1.3 \text{ GeV}$, the gluon PDF is most likely larger than the down quark distribution even at very large x . It may or may not even be larger than the up quark distribution—more data will be needed to determine that. An important challenge for further study would be to see if perhaps one can ar-

gue convincingly from models of the nonperturbative physics of the proton that “valence-like” gluon alternatives where $g(x, \mu_0) > u(x, \mu_0)$ at large x are unphysical, in which case the uncertainty in PDFs could be significantly reduced.

In Memoriam: It has been our pleasure to work with, and be inspired by, our late mentor, colleague, and friend Wu-Ki Tung. Much of the methodology of modern PDF global analysis was his innovation, and he remained involved in this work to the end of his life.

Acknowledgments

We thank D. Soper for discussions on the EKS NLO jet program. We thank Kenichi Hatakeyama for providing the CDF Run II data files. We thank M. Ubiali, A. Guffanti, S. Forte, and J. Rojo for discussions on the NNPDF approach. The revised version of the paper benefited from insightful suggestions from the anonymous referee for Phys. Rev. D.

This research was supported by the U.S. National Science Foundation under grants PHY-0354838, PHY-055545, and PHY-0757758; U.S. Department of Energy under grant DE-FG02-04ER41299; National Center for Theoretical Sciences and National Science Council of Taiwan under grant NSC-97-2112-M-133-001; and by the Lightner-Sams Foundation.

Appendix: Alternative choices for eigenvectors

Here we sketch how the eigenvector PDF sets in a global QCD analysis can be recalculated to more simply represent the uncertainty of a particular physics quantity, such as the gluon distribution at large x that is studied in this paper. See [19] for a more detailed description.

The standard Hessian method for error analysis is based on a quadratic expansion of χ^2 in the neighborhood of the minimum of a global fit. This expansion follows from Taylor series:

$$\chi^2 = \chi_0^2 + \frac{1}{2} \sum_{i=1}^N \sum_{j=1}^N \left(\frac{\partial^2 \chi}{\partial a_i \partial a_j} \right)_0 (a_i - a_i^{(0)}) (a_j - a_j^{(0)}), \quad (4)$$

where there are no first-order terms because the expansion is about the minimum, and terms higher than second order have been dropped. The $\{a_i\}$ in Eq. (4) are the parton parameters of the global fit, and quantities with superscript (0) are evaluated at the minimum of χ^2 . Formally, one can express the displacements $a_i - a_i^{(0)}$ as linear combinations of the normalized eigenvectors of the matrix of second derivatives to obtain a

diagonal expression

$$\chi^2 = \chi_0^2 + \sum_{i=1}^N z_i^2 \quad (5)$$

in which the new coordinates $\{z_i\}$ are the coefficients that multiply the eigenvectors. Because nonquadratic behavior appears at widely different scales in different directions of the parameter space, and because the second-derivative matrix must be calculated numerically by finite differences, it is necessary in practice to compute the linear transformation from coordinates $\{a_i - a_i^{(0)}\}$ to coordinates $\{z_i\}$ by a series of iterative steps [15].

The choice of eigenvectors that define the transformation to the diagonal form (5) is not unique, because any further orthogonal transformation of the parameters $\{z_i\}$ will preserve that form. This freedom to make a further orthogonal transformation can be used to simultaneously diagonalize any one additional function of the coordinates within the quadratic approximation. Specifically, if G is a function of the original coordinates, one can choose the new coordinates such that

$$G = G_0 + \sum_{i=1}^N (P_i z_i + Q_i z_i^2). \quad (6)$$

while maintaining (5). This form (6), which is accurate through second order in the $\{z_i\}$, is obtained by the following recipe: (1) Calculate the symmetric matrix $(\partial^2 G / \partial z_i \partial z_j)_0$ using the “old” $\{z_i\}$ by finite differences; (2) Express these “old” $\{z_i\}$ as linear combinations of the eigenvectors of that matrix; (3) The coefficients of these linear combinations become the desired “new” $\{z_i\}$. These steps are iterated a few times to refine the transformation. This procedure is described explicitly in [19].

In the iterative procedure used in our previous uncertainty analyses [4, 5, 22], the quantity G defining the transformation (6) was the overall length-squared of the displacement from the minimum in the space of the original shape parameters: $\sum_{i=1}^N (a_i - a_i^{(0)})^2$. To study the uncertainties of $g(x, \mu)$ at large x , we can instead choose G to be a Mellin moment of some PDF, such as $\int_0^1 x^n g(x, \mu_0) dx$ with $2 \lesssim n \lesssim 5$; or we can simply choose $G = g(x, \mu_0)$, e.g., at $x = 0.55$ as was done to create the right hand side of Fig. 6. To facilitate the study of some interesting physical quantities, one might want to choose G to be, say, the cross section for W , Z , or Higgs boson production. Another choice, which is useful for exploring the internal consistency of a global fit, is to define G as the contribution to χ^2

from a particular subset of the data. This application is the subject of [19].

-
- [1] T. Aaltonen *et al.* [CDF Collaboration], Phys. Rev. D **78**, 052006 (2008) [arXiv:0807.2204 [hep-ex]].
 - [2] V. M. Abazov *et al.* [D0 Collaboration], Phys. Rev. Lett. **101**, 062001 (2008) [arXiv:0802.2400 [hep-ex]].
 - [3] A. Abulencia *et al.* [CDF - Run II Collaboration], Phys. Rev. D **75**, 092006 (2007) [Erratum-ibid. D **75**, 119901 (2007)] [arXiv:hep-ex/0701051].
 - [4] J. Pumplin, D. R. Stump, J. Huston, H. L. Lai, P. M. Nadolsky and W. K. Tung, JHEP **0207**, 012 (2002) [arXiv:hep-ph/0201195]; D. Stump, J. Huston, J. Pumplin, W. K. Tung, H. L. Lai, S. Kuhlmann and J. F. Owens, JHEP **0310**, 046 (2003) [arXiv:hep-ph/0303013]; W. K. Tung, H. L. Lai, A. Belyaev, J. Pumplin, D. Stump and C. P. Yuan, JHEP **0702**, 053 (2007) [arXiv:hep-ph/0611254].
 - [5] P. M. Nadolsky *et al.*, Phys. Rev. D **78**, 013004 (2008) [arXiv:0802.0007 [hep-ph]].
 - [6] A. D. Martin, W. J. Stirling, R. S. Thorne and G. Watt, arXiv:0901.0002 [hep-ph].
 - [7] A. A. Affolder *et al.* [CDF Collaboration], Phys. Rev. D **64**, 032001 (2001) [Erratum-ibid. D **65**, 039903 (2002)] [arXiv:hep-ph/0102074].
 - [8] B. Abbott *et al.* [D0 Collaboration], Phys. Rev. D **64**, 032003 (2001) [arXiv:hep-ex/0012046].
 - [9] S.D. Ellis, Z. Kunszt and D. Soper, Phys. Rev. Lett. **69**, 1496 (1992).
 - [10] T. Kluge, K. Rabbertz and M. Wobisch, arXiv:hep-ph/0609285.
 - [11] Z. Nagy, Phys. Rev. Lett. **88**, 122003 (2002); Phys. Rev. **D68**, 094002 (2003).
 - [12] N. Kidonakis, J. F. Owens, Phys. Rev. D **63**, 054019 (2001). [arXiv:hep-ph/0007268].
 - [13] F. Abe *et al.* [CDF Collaboration], Phys. Rev. Lett. **77**, 438 (1996) [arXiv:hep-ex/9601008].
 - [14] J. Huston, E. Kovacs, S. Kuhlmann, H. L. Lai, J. F. Owens, D. E. Soper and W. K. Tung, Phys. Rev. Lett. **77**, 444 (1996) [arXiv:hep-ph/9511386].
 - [15] J. Pumplin, D. R. Stump and W. K. Tung, Phys. Rev. D **65**, 014011 (2001) [arXiv:hep-ph/0008191].
 - [16] R. D. Ball *et al.* [NNPDF Collaboration], Nucl. Phys. B **809**, 1 (2009) [arXiv:0808.1231 [hep-ph]].
 - [17] J. C. Collins and J. Pumplin, arXiv:hep-ph/0105207.
 - [18] P. M. Nadolsky, “Correlated systematic errors in the global QCD analysis,” Manuscript in preparation.
 - [19] J. Pumplin, “Data set diagonalization in a global fit,” [arXiv:0904.2425 [hep-ph]].
 - [20] S. Chekanov *et al.* [ZEUS Collaboration], Eur. Phys. J. C **42**, 1 (2005) [arXiv:hep-ph/0503274].
 - [21] D. Stump *et al.*, Phys. Rev. D **65**, 014012 (2001) [arXiv:hep-ph/0101051].
 - [22] J. Pumplin *et al.*, Phys. Rev. D **65**, 014013 (2001) [arXiv:hep-ph/0101032].
 - [23] J. Pumplin, A. Belyaev, J. Huston, D. Stump and W. K. Tung, JHEP **0602**, 032 (2006) [arXiv:hep-ph/0512167].
 - [24] J. Huston, J. Pumplin, D. Stump and W. K. Tung, JHEP **0506**, 080 (2005) [arXiv:hep-ph/0502080].